Chapter 8
Friction and Electrostatics

Contents

8.1 Introduction

Friction and electricity are closely related and the latter is a common outcome of the former, as much as wear. Attractive forces between rubbed solids have been noticed since ancient times and many scientists claim that *triboelectrification* (electrification by friction) is the oldest known manifestation of the electrical sciences. On the other hand, although both tribology and electrostatics are related to everyday phenomena, many basic issues are still matters of debate and did not receive much attention during most of twentieth century. However, a surge of progress has been observed in both cases for the past few decades and the mutual feedback between friction and charging is now clear.

Tribology and electrostatics are inherently complex sciences, thus it is not surprising that the their mutual relationships are also complex. The conception that

F. Galembeck, T.A.L. Burgo, *Chemical Electrostatics*,
DOI 10.1007/978-3-319-52374-3_8

friction must be related to attractive forces seems to be very intuitive: whenever two bodies are mutually attracted, it must be difficult to slide one of them over the other. In 1734, Desaguliers observed that when metals were polished, this could increase friction due to adhesive forces. However, his observations contradicted the *Amontons' law* that was then already established. This law states that friction coefficients are independent of the contact area or, in other words, friction forces are only dependent on the normal load and proportional to it. Although Desaguliers' experimental findings were correct, he could not explain why friction coefficient is independent of the contact area while adhesion is dependent.

Much later in 1950, Bowden and Tabor clarified this apparent contradiction by introducing the concept of *real contact area* that is the summation of the areas of numerous microscopic regions where asperities from both contacting surfaces form contacting junctions. These contacting sites may be more or less numerous, depending on surface roughness and they are the only sites for atom-to-atom contact [1]. These authors showed that the frictional force is strongly dependent on the real contact area and increasing the normal force also increases the number and extent of contacting sites. They could thus explain why adhesive interactions contribute to frictional forces, although real area of contact was then more a qualitative notion than a measurable property of the system.

8.1.1 Adhesive Contact Models: JKR, DMT and Maugis

In his model for mechanical contact, Hertz [2] assumed that only compressive stresses at the interface were responsible for the contact between solid elastic bodies and he found that the area of contact varies non-linearly with the normal force since it is proportional to $F^{2/3}$. At the contact zone, a pressure distribution is created that elastically deforms the interface. Moreover, this pressure distribution $p_{(r)}$ is given by Eq. 8.1. It is semielliptical over the contact area peaking at its center:

$$p_{(r)} = p_0 \left(1 - r^2 / a^2\right)^{\frac{1}{2}} \tag{8.1}$$

where a is the radius of the contact zone, r is the distance from the center of the contact to the point being considered ($r^2 = x^2 + y^2$) and p_0 is the maximum pressure. The Hertz analysis is fairly universal and routinely used in the analysis of tribology experiments. On the other hand, interactions between solids, particularly between colloidal particles, were later established as the result of interatomic forces, especially of van der Waals forces. It was then found [3] that an extra force is needed to separate two solids in close contact. Although Bowden and Tabor could experimentally verify that adhesion contributes to friction due to elasto-plastic deformations at the interface, it was only during the 70s that a great effort was made to understand the contribution made by adhesive forces to Hertzian contact.

In a very elegant work, Johnson, Kendall and Roberts [4] (JKR were capable to include elastic deformations arising from the adhesive forces to the contact equilibrium between elastic bodies. They assumed that adhesive forces (at the interface only) increase the contact area and change both penetration and stored elastic energy. So, if a tensile stress induced by pulling forces is added to Hertzian compressive stress, the total normal stress $p(r)$ at the interface is:

$$p(r) = p_0\left(1 - r^2 / a^2\right)^{\frac{1}{2}} + p_0^{'}\left(1 - r^2 / a^2\right)^{-\frac{1}{2}} \tag{8.2}$$

In the Hertzian theory, a negative value of $p_0^{'}$ was rejected because tension could not be sustained under negative loads. The first term in Eq. (8.2) is positive, while the second, the tensile stress induced by surface forces, is negative. So, in the presence of adhesive forces the tensile stress deforms the edges of the interface and consequently increases the contact area. JKR theory is especially successful with elastic bodies under low loads. On the other hand, it fails under high loads, when the experimental results are well fitted by Hertz theory. This observation suggests that short-range surface forces only become important when the normal load tends to zero, for the contact of elastic materials. The surface stress distribution predicted by Eq. (8.2) is such that stress goes to infinity at the edge of the interface. On the other hand, this very high stress is predicted but not observed, because JKR theory implicitly assumes that surface forces act over an infinitesimally small distance exactly at the interface and not outside the contact area [5].

Both theory and successful verification of the original JKR theory are based on short-range attractive forces and it is thus especially valid for smooth surfaces with low elastic modulus because these short-range surface forces are not significant at distances exceeding some nanometers. Moreover, soft materials (in the original work the authors used rubber over gelatin) can be flattened to fill in asperities, forming a very intimate interface. On the other hand, for more realistic conditions as when the interface is not much deformed and materials are sufficiently rigid, the stress profile can be assumed as Hertzian.

In fact, Derjaguin, Muller and Toporov [6] (DMT) realized that for rigid materials, adhesive forces cannot overcome elastic modulus and consequently the interface is not the result of deformed surfaces. Then, adhesive forces are taken into account but they must be computed outside the contact area so that the normal load is the result of the external load and the adhesion force. In practice, the adhesive force measured with an indenter is:

$$F_{(\text{adhesion})} = 2\pi RW \tag{8.3}$$

where R is the spherical indenter radius (for a sphere-on-flat geometry) and W is the work of adhesion. $F_{(\text{adhesion})}$ is then added to the Hertz contact equation (Eq. (8.1)). Many practical situations fit well within DMT theory. For instance, the Quantitative Nanomechanical mode (QNM®) of AFM, recently developed by Bruker, uses the

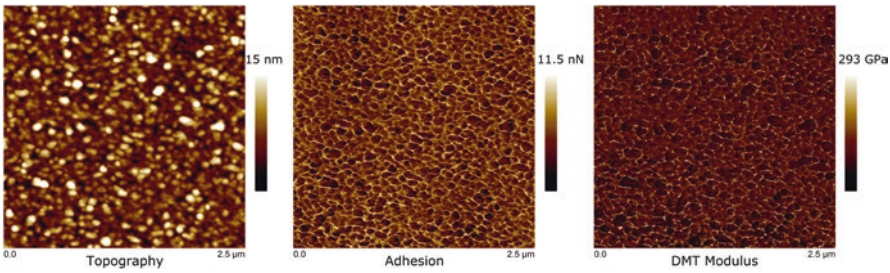

Fig. 8.1 Application of DMT theory. Quantitative nanomechanical mode (QNM) for plasma-deposited nickel nitride (Ni-N) film. The Young modulus is calculated from *DTM analysis*

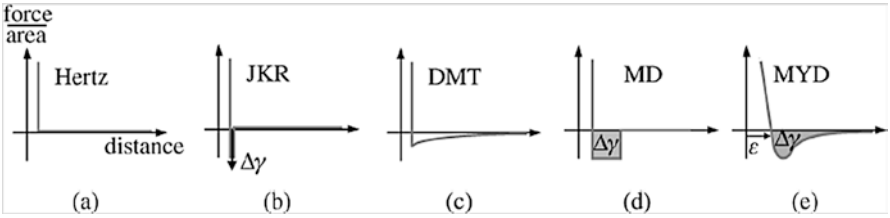

Fig. 8.2 Description of contact mechanics models. While the Hertz model does not consider the adhesion in contact, the JKR model includes only a short-range adhesion in the contact area and is a function of the work of adhesion $\Delta\gamma$. The DMT model shows a long-range surface forces and the Maugis-Dugdale (MD) model considers the square well potential to describe attractive forces. The Muller, Yushenko and Derjaguin (MYD) uses a Lennard-Jones potential to include both the short-range and long-range forces. Reprinted with permission from [10]

DTM theory to calculate the Young modulus of materials during force-curve measurements. Figure 8.1 shows the topography, adhesion and DMT modulus mappings for a plasma deposited nickel-nitrate (Ni-N) film. The adhesion mapping is obtained from pull-off force. On the other hand, the Young modulus is obtained by fitting the retract curve to the DMT model. Note that in Fig. 8.1, most regions where adhesion is high also show a high DMT modulus, as well.

Although controversy and heated debates on the applicability of both theories were entertained for some years, Tabor [7] realized that the two theories represent the opposite extreme cases of mechanical contact: JKR is more applicable to large radius, compliant solids with strong adhesion while DMT is more indicated for small radius, rigid solids with low adhesion. Later, using a Dugdale (square well) potential model to describe attractive forces, Maugis [8] derived analytical solutions to show the transition between both theories and he was capable to handle intermediate cases. Figure 8.2 shows a comparison between some important models. In practice, the Hertz analysis and JKR-DMT theories are the most used models

because they use simple equations relating the normal stress with the radius of the contact zone. For more precise work, the Maugis-Dugdale (MD) or even the Muller, Yushchenko and Derjaguin (MYD) model [9] (which describes the adhesion force via Lennard-Jones potential) can be used [10].

There are many articles and books where all derivations of the above-mentioned models and equations can be found in detail. In this chapter, we only describe briefly the main features of the most widely used theories to contextualize tribocharging within the main problems in contact mechanics.

Study in this area produced outstanding results of the direct measurement of van der Waals forces acting between surfaces, thanks to the famous Surface Forces Apparatus (SFA) developed by Tabor, Winterton and Israelachvili in the early 1970s.

At this point, it is worth stressing that *friction* does not correlate directly with *adhesion*. This seems contradictory, but there are many examples of bodies with high friction coefficients but having low adhesive forces, and vice versa. On the other hand, since friction is an energy-dissipation process it actually relates well to *adhesion hysteresis* [11], a concept introduced by Israelachvili [12]: the work required to separate two surfaces is typically greater than the work done when contacting them. Adhesion hysteresis is the difference between both and friction can be predicted from the adhesion hysteresis curve.

8.2 From Macro to Nanoscale

For macroscopic objects, forces such as gravity tend to be more significant than those forces (van der Waals or Coulombic) that arise from intermolecular interactions. Also, friction has many factors other than surface forces, like cohesion, roughness, viscoelasticity, hardness, lubricated conditions, elasto-plastic deformability and perhaps still others.

The basic laws of friction established by Amontons and Coulomb are three empiric laws:

first law: friction is proportional and perpendicular to the normal load;
second law: friction is independent of the apparent contact area;
third law: kinetic friction is independent of sliding velocity.

Although these laws may appear simplistic and they are not derived from fundamental principles, they are extremely valuable for solving real life problems. Moreover, the relationships stated by these laws are the result of many important interfacial, molecular and materials phenomena that are by themselves rather complex or not fully understood.

Amontons already noticed that uneven surfaces have higher friction coefficients than smooth surfaces. Roughness is thus an important variable that lead many authors to think that friction was originated only from roughness and nothing else.

On the other hand, after Bowden and Tabor introduced the concept of real contact area, the comprehension of friction phenomena reached a higher level. Today, it is accepted that friction has two basic factors [5]:

1. The *adhesion force* needed to overcome attractive interactions developed through the outermost parts (tips of the asperities) of the surfaces;
2. The *plowing force* that is observed when one surface is significantly harder than the other. In this case the softer surface is plowed by the asperities on the harder one [13].

Friction force can be written as:

$$F = F_{\text{adhesion}} + F_{\text{plowing}} \tag{8.4}$$

Both adhesion and plowing force are by themselves the result of many important surface phenomena. Attractive interactions (van der Waals forces), mechanical shearing, elasto-plastic deformations, contaminants, water adsorption, cohesion (weakly bound layers [14]), and presence of third bodies [15] (material transfer) are only some of many factors that can influence the adhesion and plowing forces. On the other hand, at the nano (or micro) scale surface forces can overcome many of the energy dissipating mechanisms so as to become more important than these as well as gravity.

Progress in the relevant instrumentation, SFA and AFM allowed the demonstration of the importance of coulombic interactions between surfaces to friction across interfaces under relative motion, at the microscopic level.

Salmeron and collaborators applied bias voltage to a *n*-type Si(100) wafer with stripes of highly B-doped p-type semiconductor, to control friction forces measured while passing the AFM tip over the wafer surface. They could thus change friction as the result of interactions between excess charge in the wafer and the tip [16, 17].

Reduction of friction forces on high-temperature superconductors was achieved due to the underlying atomic-scale electronic and phononic mechanisms [18, 19]. Instead, when the resulting forces across the interface are attractive, friction is raised and persists even under negative loads [20].

It is expected that forces from asymmetric fluctuating electric fields that are formed as the result of triboelectrification of moving bodies dissipate energy by dragging charge along the surface and thus increasing friction losses [21]. This statement has not yet been experimentally proven.

8.3 Electrostatic Contribution to Friction

Coulombic interactions are long-range forces that extend farther than other surface forces. Usually, van der Waals forces do not extend beyond few tens of nanometers falling as d^{-7} with the separation distance, d. On the other hand, electrostatic forces

are felt even at macroscopic distances and they should not continue to be neglected in contact mechanics and friction. Considering that the electrostatic field developed at dielectric interfaces can be as high as to produce air dielectric breakdown, static electricity effects must be included in comprehensive atomic-scale treatment of friction, especially when insulating materials are involved.

The only explanation for the current neglect of Coulombic interactions in friction is the enormous complexity introduced by considering electrostatic forces. First, there is still a widespread lack of understanding of the mechanisms and patterns of electrostatic charging of materials, at the atomic-molecular level, that is discussed in other chapters in this book. Also, electrostatic interactions at the solid–gas interface are strongly dependent on many ambient factors, including its water content [22] that in turn depends on the relative humidity. Moreover, even approximate amounts of charge carriers formed or exchanged during contact are hardly known, when one of the contacting bodies is an insulator [23].

Nakayama and collaborators [24] have shown that the extremely intense electric fields generated due to tribo-physical and –chemical phenomena produced by sliding contacts create sites with high energy density, where a *triboplasma* is formed. A spectacular demonstration of the formation of high-energy species was made by the Putterman group, showing the emission of Bremsstrahlung X-rays [25] produced under intense electric fields that were in turn the result of surface charging by breaking adhesive bonds.

Budakian and Putterman investigated the effect of charge transfer in stick-slip friction at metal–insulator interfaces [26]. They found that charge transfer accompanying the slip events is proportional to the force jumps, pointing toward a common origin for triboelectrification and friction, at least in their system. The effect of triboelectricity on friction coefficients of metals was also demonstrated in different systems [27–29] but not in insulator–insulator interfaces, where quantitative information on the amount of charge and its distribution is hardly available.

8.3.1 Macro Experiments Relating Surface Charge and Friction Coefficients

Surprisingly, the effect of triboelectricity on friction coefficients was only recently quantified, for two dielectric solids at the macroscale and under well-defined conditions. This was only possible when the author's group had already accumulated 15 years of experience in the investigation of electrostatic charging of materials, including techniques for potential and charge mapping from the nano- to the macroscale [22].

This allowed the production and assessment of insulator surfaces with fairly uniform charge density [22, 30]. Sliding felt wool over a PTFE sheet produces negatively charged surfaces with lower local variations than most other systems. Half-life for potential decay in these surfaces is in the range of a few days so that samples can

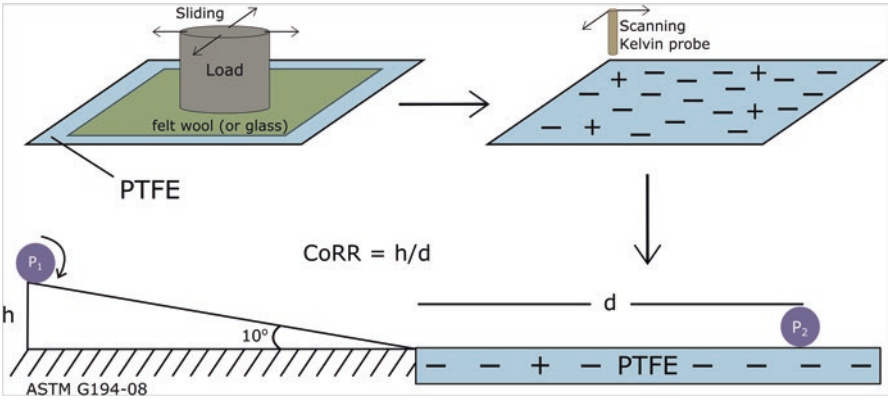

Fig. 8.3 Coefficient of rolling resistance on tribocharged surface setup. PTFE was supported on an aluminum holder and rubbed with felt wool (14 × 14 cm^2) with pressure adjusted to 1.0 ± 15 kPa that was slid for 4 cm at the speed of 1 cm s^{-1}. CoRR measurements followed the ASTM Standard (G194-08)

be prepared, and surface static potential distribution can be mapped. Most uniform samples covering a range of charge densities are thus selected for friction measurements, as shown in Fig. 8.3.

The experiments to determine the coefficient of rolling resistance (CoRR) of glass beads on PTFE as a function of the electrostatic potential in the latter (previously mapped with a Kelvin probe) are straightforward: glass beads are placed at a chosen height (in this case, h = 1.25 mm) on an aluminum smooth ramp with a suitable inclination angle (10°) and then allowed to roll down onto a flat tribocharged PTFE surface. The distance roamed by each sphere on the PTFE surface, d, is used to calculate the coefficient of rolling resistance, CoRR = h/d.

Figure 8.4 shows that rolling friction of glass spheres increases with electrostatic potential on charged PTFE surfaces [31]. The electrostatic potential goes from values close to 0 V to −3300 V in the various samples (Fig. 8.4a). Neutral glass spheres released from height h roll over charged PTFE but they quickly stop, after moving for only a fraction of the distance observed in uncharged PTFE. This shows that charge on the films introduces a powerful mechanism for mechanical energy dissipation. These experiments allow the calculation of the coefficient of rolling resistance (CoRR), as shown in Fig. 8.1b, as a function of the average potential on the film. CoRR increases many-fold in charged PTFE, in a potential range that is easily achieved by rubbing this polymer with glass and other common materials.

The effect of tribocharging on sliding friction was examined by sliding polyethylene (PE) pellets on PTFE film, when they are immobilized by triboelectrification. The experimental setup can be seen in Fig. 8.5: PE pellets were randomly placed on PTFE surface and shaken on a reciprocating table for 5 min. Then, the holder

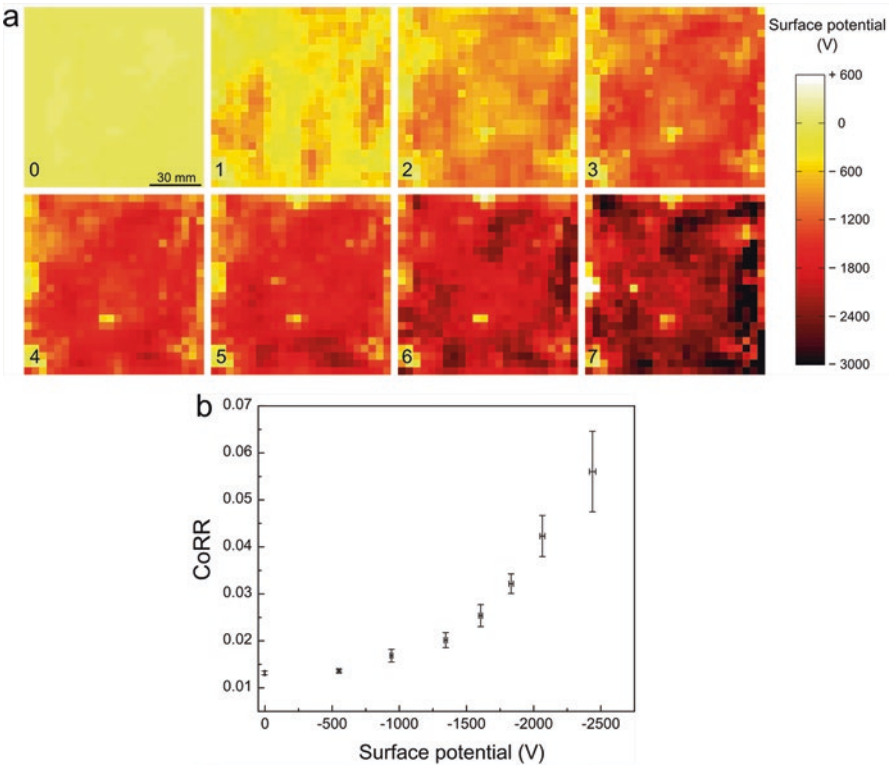

Fig. 8.4 Determination of CoRR of glass beads rolling on tribocharged PTFE surfaces. (**a**) The potential map for each plate used. (**b**) CoRR vs. average surface potential of tribocharged PTFE plates. Vertical error bars are mean standard deviations from ten replicate measurements while the horizontal bars are standard deviations of average potential for all the pixels on each plate. Reprinted with permission from [31]

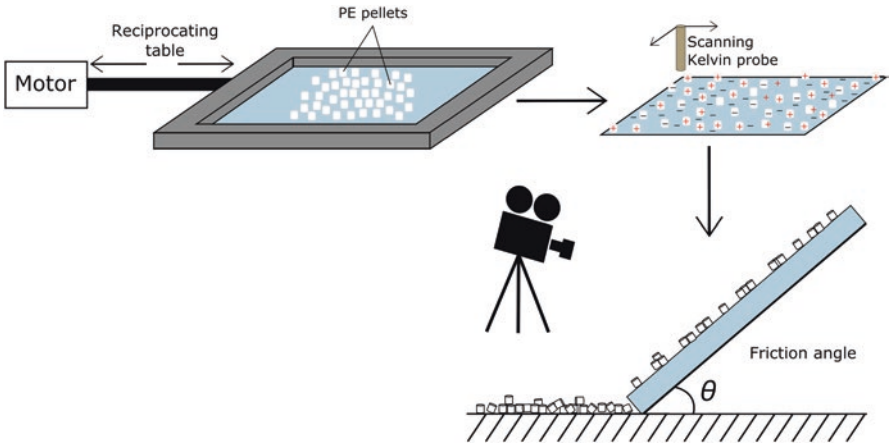

Fig. 8.5 Friction angle on tribocharged surfaces setup. Uncharged PTFE sheets framed on a thick aluminum sheet, carrying 30 PE pellets randomly placed on its surface were shaken for 5 min on a reciprocating table and then mounted on the swinging arm of the inclined plane, gradually raised in 5° steps and the number of pellets sliding at each angle was recorded

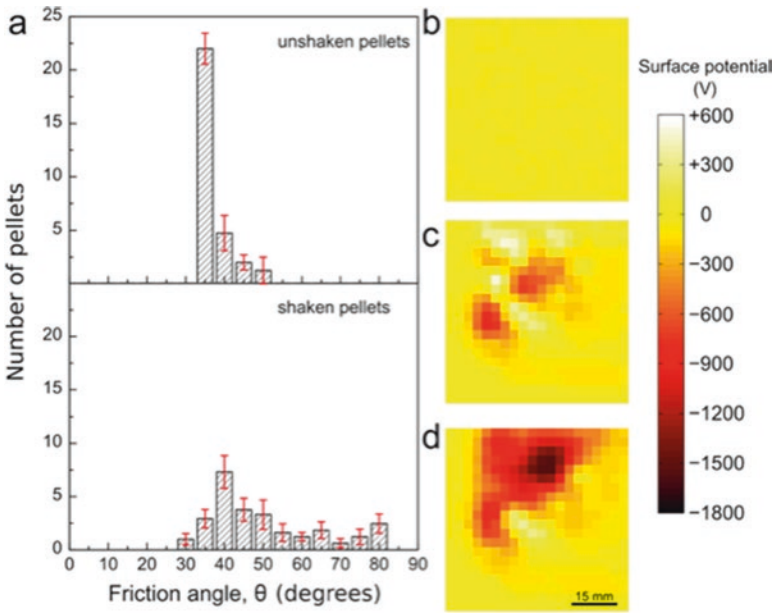

Fig. 8.6 Tribocharging effect on friction angles of PE pellets on PTFE. (**a**) Control measurement using unshaken pellets (*top*) and the distribution of values obtained by averaging the results of 13 shaking runs using 30 pellets each (*bottom*). Potential maps of: (**b**) PE pellets on clean PTFE prior to shaking, (**c**) pellets shaken for 300 s on PTFE and (**d**) PTFE after removal of PE pellets. Error bars are standard deviations of the average. Reprinted with permission from [31]

supporting the PTFE film and the pellets was mounted on the swinging arm of an inclined plane that was gradually raised in 5° steps, while recording the number of pellets sliding at each angle. Static friction coefficients $\mu_s = \tan\theta$ were then calculated and the histograms of pellet number vs. sliding friction angle are in Fig. 8.6. Friction angles of uncharged PE pellets over PTFE peaks at 40° but for the tribocharged pellets they spread toward much higher and also to lower angles (>90° down to 30°), after a short sliding time. This shows that tribocharging produces very large friction coefficients but some pellets have *lower* friction coefficients than the neutral ones.

In these experiments, the electrostatic measurements were done ex-situ, apart from the friction measurements. Thus, they do not give a real-time perspective on charge exchange and friction modification. Burgo and Erdemir [32] overcame this issue by doing in-situ experiments where charge exchange is measured online, concurrent with friction measurements. They used a rigorous setup in tribology, *the ball-on-disk* geometry, to record the macroscopic friction force while simultaneously measuring the current generated at the metal–insulator interface, as shown in Fig. 8.7. The results pointed out to a strong correlation between the macroscopic

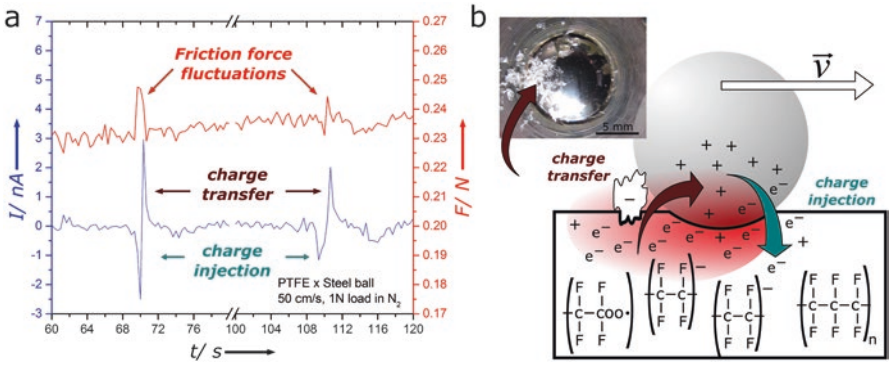

Fig. 8.7 Tribocurrent at metal–insulator interfaces. (**a**) Friction force fluctuations and tribocurrent generation at the metal–PTFE interface and (**b**) schematic representation of the underlying mechanism. Reprinted with permission from [32]

friction force and the electrostatic charge exchange at the interface. Figure 8.7a shows friction force and tribocurrent that were recorded simultaneously by sliding a steel ball on a PTFE surface under nitrogen atmosphere. The tribocurrent signal is always accompanied by a transient increase in the friction force signal, producing stick-slip behavior, as schematically described in Figure 8.7b.

Friction force fluctuations are often observed in tribological tests and Singer et al. have shown that this effect is generally caused by the presence of third bodies [15]. The micrograph in Fig. 8.7c was acquired after the tribological experiments and it shows macroscopic flake residues of PTFE adherent to the metallic surface, but only on the "*tail*" of the sphere, which means that the PTFE sticks to metal right after the ball slips on the surface. In fact, material transfer has also been pointed out as playing a key role in triboelectrification [23] and here we can state that friction force fluctuations are always followed by two tribocharging steps: first, an extra flow of electric charge from the ball to PTFE and then back. This can be understood recalling that during mechanical stress, electrons flow from compressed regions to extended ones, so that the Fermi level remains the same [33–35]. Consequently, extended regions have a negative charge density, when electrons are injected on PTFE, evidenced by the negative signal of the electric current. On the other hand, PTFE (which has a tendency to acquire negative potential in contact electrification) transfer negative charge back to the metal ball, mostly by material transfer and producing the positive current signal measured by the electrometer. Van der Waals and Coulombic interactions operate at the interfaces while chemical reactions also take place during the displacement of the metal ball on PTFE. Together, they change the contact area, reflecting directly on the macroscopic friction force.

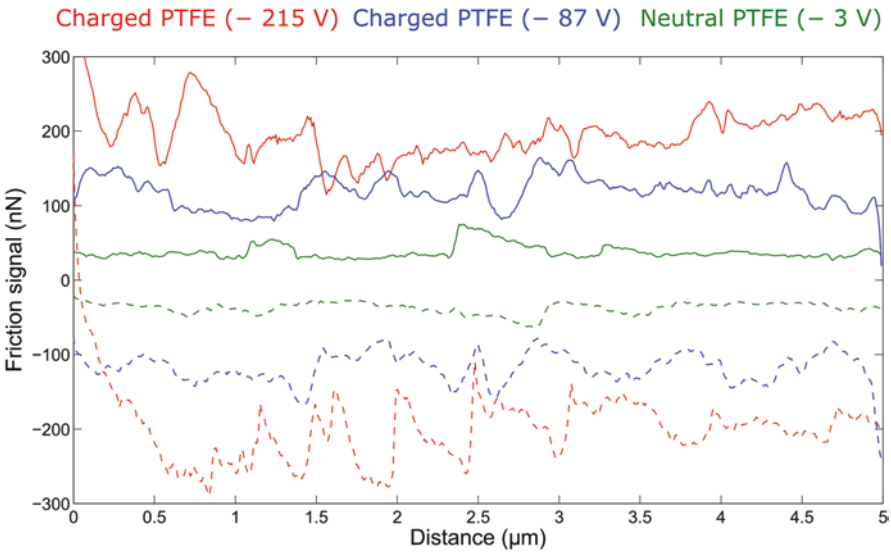

Fig. 8.8 Friction force signal on neutral and tribocharged PTFE. Friction signal profiles were extracted from FFM images. Reprinted with permission from [31]

8.3.2 AFM Experiments (LFM, Force-Distance and Nanomechanical Mode)

Tribocharge patterns are fractal [36] and they should thus display symmetry of scale. For this reason, the influence of electrostatic charge on friction should be observed at any scale, including the nanometric range. This assumption was experimentally verified using AFM in many modes and at least two different equipment configurations. Friction force microscopy (FFM) that is also called lateral force microscopy (LFM) has been invaluable in providing friction data with high spatial resolution. This technique is derived from contact mode imaging and it measures the lateral bending of the cantilever probe as it scans a surface. Results of FFM measurements on tribocharged surfaces are in Fig. 8.8, showing that the lateral force is close to zero on uncharged PTFE but it largely increases when the polymer surface is previously tribocharged. Compared to neutral PTFE, the friction signal increases roughly sevenfold when PTFE is tribocharged. A consequence of this result is that tribocharged PTFE is no longer a low surface energy material but it becomes a high surface energy solid, easily sticking to other materials.

Actually, the effect of electric charge on adhesive forces is better viewed with force vs. distance (*Fd*) curves and adhesion maps that are conveniently recorded using the PeakForce Quantitative Nanomechanical mode (PKQNM) [37]. Fd curves yield information on surface interactions, adhesion, elasto-plastic and many

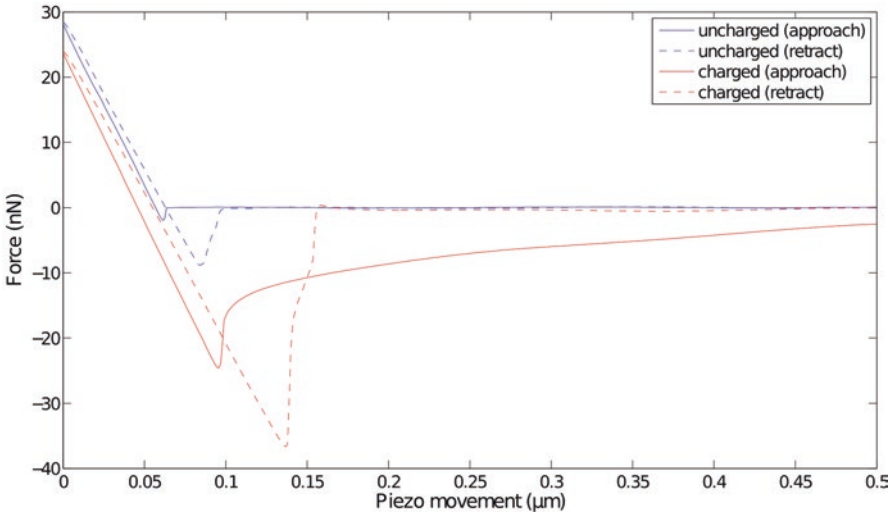

Fig. 8.9 Force–distance curves on neutral and tribocharged PTFE. Fd curves for approach and retraction of a silicon nitride tip from neat, uncharged PTFE and tribocharged PTFE. Average potential measured over the polymer with a macroscopic Kelvin electrode is −192 V. Reprinted with permission from [31]

other properties, which makes this a fundamental tool in surface science. Again, the results for neutral and previously tribocharged PTFE are markedly different. *Fd* curves [31] seen in Fig. 8.9 show that tip interaction with neutral PTFE is negligible until a short distance is attained and van der Waals attraction is observed. On the other hand, when PTFE is electrostatically charged, tip attraction during tip approach is observed at distances greater than 500 nm. Also, the pull-off force (or *adhesion force*) increase by at least a factor of 5, close to the change measured for friction signal.

The nanomechanical mode (PKQNM) has been successfully applied to the study of complex polymeric structures and relevant biological systems. PKQNM images are composed by acquiring a large number of Fd curves (commonly, 3 Fd curves per pixel) using the tapping mode in an AFM instrument. Thus, one of its capabilities is to provide adhesion maps and this was applied to explore surface properties of PTFE rubbed with a metal ball, as in the ball-on-disk tribology experiments. As seen in Fig. 8.10, the adhesive force on clean PTFE is less than 10 nN, but the adhesion on tribocharged PTFE reaches 150 nN in most pixels, due to electrostatic charge. This force range is the same as that observed for high-energy surface materials or even in geckos [38], explaining why charged PTFE strongly sticks to other materials [32].

Thus, Coulombic interactions due to surface charge may supersede all other contributions to macro and micro friction coefficient, at the macro and nanoscales.

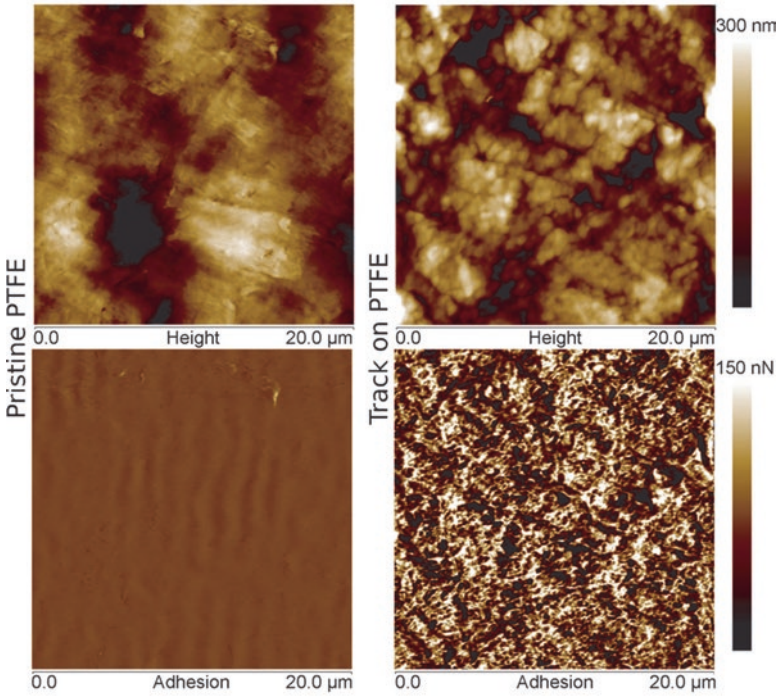

Fig. 8.10 Adhesion maps on neutral and rubbed PTFE. Topography (*top*) and adhesion (*bottom*) maps of pristine and tribotested (N_2, 2 N load, and 50 cm s^{-1}) PTFE obtained using the PeakForce Quantitative Nanomechanical mode (PKQNM). Reprinted with permission from [32]

This raises a new question: *How can the electrostatic charge be included in models for contact mechanics? Is it possible to add a Coulombic force contribution, simply?* To answer this question, we need to recall that details of contact electrification are still poorly known, in almost every dielectric material; there are even large differences between single contact, multiple contacts and sliding contact (rubbing) [35]. Also, when an insulator is part of the interface there is an inherent unpredictability [39], due to the chaotic nature of the micro [40] and macro [30] mosaics of charge developed during contact electrification. So, the answer to this question cannot be highly positive for every material, at the present time.

A Coulombic force contribution can be added in the cases of metals or semiconductors, when charge transferring follows work function properties and surface charge density is expected to be uniform. However, neither overall charge or charge density are more or less easily calculated for dielectrics and they can only be obtained from experimental measurements. So, the introduction of charging effects on contact mechanics experiments depends on previously acquiring the surface

electrostatic maps (with macroscopic or microscopic Kelvin probes) and then using these samples in contact experiments, designed to minimize further charging or charge pattern modification. At this point, this seems to be the only way to proceed. Beyond, it is necessary to recall that most metal surfaces are coated with some oxide that is often a dielectric itself. So, even for metals strong fluctuations of charge density are to be expected.

8.4 Conclusions

There is a powerful interplay between friction and tribocharging: friction produces surface charge that in turn modifies friction coefficients that in turn affect friction forces. These mutual effects are mediated by chemical reactions added to mass transfer among the surfaces in contact. Moreover, tribocharge in dielectrics follows complex, fractal geometrical patterns that make its effects on friction quite complex. For this reason, they can only be assessed by well-designed experiments, in the absence of established theories. The mutual effects of friction and surface charge are certainly relevant to contact mechanics and materials wear but surface charge is not included in the relevant theories. Its inclusion is highly desirable but it will not be an easy task.

References

1. Bowden FP, Tabor D (1954) Friction and lubrication. Oxford University Press, Oxford
2. Hertz H, Reine J (1882) Ueber die Berührung fester elastischer Körper. Angew Math 92:156–171
3. Adamson AW, Gast AP (1997) Physical chemistry of surfaces. Wiley, New York
4. Johnson KL, Kendall K, Roberts AD (1971) Surface energy and the contact of elastic solids. Proc R Soc A Math Phys Eng Sci 324:301–313
5. Mate CM (2008) Tribology on the small scale: a bottom up approach to friction, lubrication, and wear. Oxford University Press, Oxford
6. Derjaguin BV, Muller VM, Toporov YUP (1975) Effect of contact deformation on the adhesion of particles. J Colloid Interf Sci 53:314–326
7. Tabor D (1977) Surface forces and surface interactions. J Colloid Interf Sci 58:2–13
8. Maugis D (1992) Adhesion of spheres: the JKR-DMT transition using a Dugdale model. J Colloid Interf Sci 150:243–269
9. Muller VM, Yushchenko VS, Derjaguin BV (1980) On the influence of molecular forces on the deformation of an elastic sphere and its sticking to a rigid plane. J Colloid Interf Sci 77:91–101
10. Shi X, Zhao Y-P (2004) Comparison of various adhesion contact theories and the influence of dimensionless load parameter. J Adhes Sci Technol 18(1):55–68
11. Chen YL, Israelachvili JN (1991) Molecular mechanisms associated with adhesion and contact angle hysteresis of monolayer surfaces. J Phys Chem 95:10736–10747
12. Yoshizawa H, Chen YL, Israelachvili J (1993) Fundamental mechanisms of interfacial friction. 1. Relation between adhesion and friction. J Phys Chem 97:4128–4140

13. Tabor D (1995) Tribology—the last 25 years. A personal view. Tribol Int 28(1):7–10
14. Mittal KL (1976) Adhesion aspects of metallization of organic polymer surfaces. J Vac Sci Technol 13:19–25
15. Singer IL, Dvorak SD, Wahl KJ, Scharf TW (2003) Role of third bodies in friction and wear of protective coatings. J Vac Sci Technol A 21:232–240
16. Park JY, Ogletree DF, Thiel PA, Salmeron M (2006) Electronic control of friction in silicon pn junctions. Science 313:186–186
17. Park JY, Qi Y, Ogletree DF, Thiel PA, Salmeron M (2007) Influence of carrier density on the friction properties of silicon pn junctions. Phys Rev B 76:064108
18. Altfeder I, Krim J (2012) Temperature dependence of nanoscale friction for Fe on YBCO. J Appl Phys 111:094916
19. Krim J (2012) Friction and energy dissipation mechanisms in adsorbed molecules and molecularly thin films. Adv Phys 61:155–323
20. Brezoczky B, Seki H (1990) Triboattraction: friction under negative load. Langmuir 6:1141–1145
21. Park JY, Salmeron M (2014) Fundamental aspects of energy dissipation in friction. Chem Rev 114:677–711
22. Burgo TAL, Rezende CA, Bertazzo S, Galembeck A, Galembeck F (2011) Electric potential decay on polyethylene: role of atmospheric water on electric charge build-up and dissipation. J Electrostat 69:401–409
23. McCarty LS, Whitesides GM (2008) Electrostatic charging due to separation of ions at interfaces: contact electrification of ionic electrets. Angew Chem Int Ed 47:2188–2207
24. Matta C, Eryilmaz OL, De Barros Bouchet MI, Erdemir A, Martin JM, Nakayama K (2009) On the possible role of triboplasma in friction and wear of diamond-like carbon films in hydrogen-containing environments. J Phys D Appl Phys 42:075307
25. Camara CG, Escobar JV, Hird JR, Putterman SJ (2008) Correlation between nanosecond X-ray flashes and stick–slip friction in peeling tape. Nature 455:1089–1092
26. Budakian R, Putterman SJ (2000) Correlation between charge transfer and stick-slip friction at a metal-insulator interface. Phys Rev Lett 85:1000–1003
27. Akbulut M, Godfrey Alig AR, Israelachvili J (2006) Triboelectrification between smooth metal surfaces coated with self-assembled monolayers (SAMs). J Phys Chem B 110(44): 22271–22278
28. Morris S, Wood RJK, Harvey TJ, Powrie HEG (2003) Electrostatic charge monitoring of unlubricated sliding wear of a bearing steel. Wear 255:430–443
29. Seto T (1995) Effects of an electric field on the static friction of a metal on a ferroelectric material. Appl Phys Lett 67:442–443
30. Burgo TAL, Ducati TRD, Francisco KR, Clinckspoor KJ, Galembeck F, Galembeck SE (2012) Triboelectricity: macroscopic charge patterns formed by self-arraying ions on polymer surfaces. Langmuir 28:7407–7416
31. Burgo TAL, Silva CA, Balestrin LBS, Galembeck F (2013) Friction coefficient dependence on electrostatic tribocharging. Sci Rep 3:2384
32. Burgo TAL, Erdemir A (2014) Bipolar tribocharging signal during friction force fluctuations at metal-insulator interfaces. Angew Chem Int Ed 53:12101–12105
33. Harper WR (1967) Contact and frictional electrification. Oxford at the Clarendon Press, London
34. Lowell J, RoseInnes AC (1980) Contact electrification. Adv Phys 29(9):947–1023
35. Lacks DJ, Sankaran RM (2011) Contact electrification of insulating materials. J Phys D Appl Phys 44(45):453001
36. Santos JP, Corpart P, Wong K, Galembeck F (2004) Heterogeneity in styrene- butadiene latex films. Langmuir 20:10576–10582
37. Pittenger B, Erina N et al (2012) Quantitative mechanical property mapping at the nanoscale with Peak Force QNM. Bruker Application Note #128, Bruker Nano Surfaces Divison Santa Barbara, USA

38. Geim AK, Dubonos SV, Grigorieva IV, Novoselov KS, Zhukov AA, Yu Shapoval S (2003) Microfabricated adhesive mimicking gecko foot-hair. Nat Mater 2(7):461–463
39. Lacks DJ (2012) The unpredictability of electrostatic charging. Angew Chem Int Ed 51:6822–6823
40. Baytekin HT, Patashinski AZ, Branicki M, Baytekin B, Soh S, Grzybowski BA (2011) The mosaic of surface charge in contact electrification. Science 333:308–312